Available online at www.sciencedirect.com

ScienceDirect

Procedia IUTAM 14 (2015) 553 – 562

Procedia IUTAM

www.elsevier.com/locate/procedia

IUTAM_ABCM Symposium on Laminar Turbulent Transition

Investigation of the global mode in swirling combustor flows: experimental observations and local and global stability analysis

S. Terhaar[a,*], P. Paredes[b], K. Oberleithner[a], V. Theofilis[b], C. O. Paschereit[a]

[a] *Chair of Fluid Dynamics, Hermann-Föttinger-Institut, Technische Universität Berlin, Müller-Breslau-Str. 8, 10623 Berlin, Germany*
[b] *School of Aeronautics, Universidad Politecnica de Madrid, Pza. Cardenal Cisneros 3, E-28040 Madrid, Spain*

Abstract

Self-excited helical flow oscillations are frequently observed in gas turbine combustors. In the present work a new approach is presented tackling this phenomenon with stability concepts. Three reacting swirling flows are investigated. All of them undergo vortex breakdown, but only two of them show self-excited global flow oscillations at well-defined frequencies. The oscillations feature a precession of the vortex core and synchronized Kelvin-Helmholtz instabilities in the shear layers. Based on the mean flow fields, local and global linear hydrodynamic stability analyses are carried out. The dampening effect of the Reynolds stresses is accounted for by an eddy viscosity estimated from the experimental results. Both the local and the global analysis successfully identify linear global modes as being responsible for the large-scale flow oscillations and successfully predict their frequency. However, only the global analysis accurately predicts a globally stable flow field for the case without the oscillation, while the local analysis overpredicts the global growth rate. The predicted spatial distribution of the amplitude functions agree very well to the experimentally identified global mode. This successful application of global and local stability concepts to a complex and practically relevant flow configuration paves the way for the application of theoretically-founded passive and active control strategies.

Selection and peer-review under responsibility of ABCM (Brazilian Society of Mechanical Sciences and Engineering)

Keywords: Turbulent swirling flow; global mode; local and global stability analysis; eddy viscosity

1. Introduction

Swirling flows are employed in the majority of modern gas turbine combustors for aerodynamic flame stabilization. The strong swirl leads to vortex breakdown and large regions of reversed flow. The high turbulence intensity and the continuous upstream transport of hot combustion products are vital for the flame anchoring and its stability[1]. In comparison to other flame-holding techniques, such as bluff bodies, the great advantage of swirl-stabilized flames is that no combustor parts are in the direct vicinity of the flame and need to be extensively cooled.

However, the flow field topology of a strongly swirling jet is very complex and swirling flows are often prone to self-excited flow oscillations that are manifested in large-scale helical flow structures. It is frequently observed that

* Corresponding author. Tel.: +49-30-314-29798 ; fax: +49-30-314-22101.
E-mail address: steffen.terhaar@tu-berlin.de

Selection and peer-review under responsibility of ABCM (Brazilian Society of Mechanical Sciences and Engineering)
doi:10.1016/j.piutam.2015.03.079

the vortex center is dislocated from the geometrical center and precesses around it with a well-defined frequency that is of the order of the solid body rotational frequency of the flow. Synchronized to this precessing vortex core (PVC), helical Kelvin-Helmholtz instabilities are excited in the shear layers between the jet and the recirculation zones. The PVC has been observed in most strongly swirling isothermal flows but also in some reacting swirling flows[1]. If the PVC is excited, it plays an important role for the mixing processes in the shear layers[2,3] and causes large-scale heat release fluctuations[4,5,6,7]. Thus, the understanding of the PVC and the associated Kelvin-Helmholtz instabilities is of great importance for the design of combustion systems.

In the literature the effect of combustion on the flow instability was reported very ambiguously. Cases were reported, where the instability remained[7,8,2], was suppressed[9,10], enhanced[11], or where the suppression depended on the operating conditions[12,13]. The governing mechanisms for the damping of the PVC were suggested to be the increased viscosity[9,14] and low tangential velocities near the centerline[11]. Recently, experimental results within the authors' group[13] suggested the important role of the density field.

The main idea of the present work is to use linear stability theory to investigate the mechanisms involved in the excitation of the PVC. This concept has been employed so far mainly to isothermal swirling jets, where the PVC was interpreted as an unstable global mode triggered by an inherent flow resonance[15,16,17]. Recently, the local linear stability concept was also applied to realistic reacting swirling combustor flows by authors of the present study[18,19]. The analyses were able to qualitatively predict the excitation of the PVC and the mechanisms involved into its suppression. The strong influence of the density gradient was confirmed by Oberleithner et al.[18]. Terhaar et al.[19] identified in a parametric study, employing model profiles, the relation of the backflow intensity to the density gradients as the dominant parameter for the excitation of the PVC. While the prediction of the frequencies showed a good agreement, the complete suppression of the PVC in one of the investigated cases could not be predicted correctly by the local analysis.

The present paper significantly extents the preceding works[18,19] in two ways. First, a novel Newtonian eddy viscosity model is implemented into the stability analysis. And second, the local analysis is complemented by a global analysis, where the strong non-parallelity of the flow field is accounted for. The results of this study allow for new insight into the excitation mechanisms of the PVC. At the same time the comparison to detailed experimental results allows for an assessment of the capabilities and limitations of the local and global stability concept for reacting swirling jets.

The remainder of this paper is structured as follows: First, the theoretical methods, namely the triple decomposition, the proper orthogonal decomposition, and the local and global stability analysis are presented. Next, the experimental setup and the experimental results are presented. The experimental results serve as the basis for the assessment of the results of the local and global analysis in the results section.

2. Theoretical methods

In the present work the occurrence of the PVC is experimentally and analytically investigated. The cornerstone for the analysis of coherent structures in highly turbulent flows is the triple decomposition concept[20]. The time and space dependent flow $\mathbf{v}(\mathbf{x},t)$ is decomposed into a time-averaged part $\mathbf{V}(\mathbf{x})$, a part representing the coherent fluctuations (such as the PVC) $\mathbf{v}^c(\mathbf{x},t)$, and a randomly fluctuating (stochastic) part $\mathbf{v}^s(\mathbf{x},t)$

$$\mathbf{v}(\mathbf{x},t) = \mathbf{V}(\mathbf{x}) + \mathbf{v}^c(\mathbf{x},t) + \mathbf{v}^s(\mathbf{x},t). \tag{1}$$

In the present work the interest is placed on the coherent fluctuations $\mathbf{v}^c(\mathbf{x},t)$. These fluctuations can be empirically extracted from experimental measurements or analytically modeled. Both approaches are employed in this work and will be presented in the following.

2.1. Empirical mode construction using the POD

The aim of the empirical mode construction is the extraction of the coherent velocity fluctuations from measured turbulent velocity fields. For this task, the proper orthogonal decomposition (POD) is a well-established technique in fluid mechanics[21]. The POD consists of the projection of N measured (or simulated) velocity fields on an orthogonal

N-dimensional vector base that maximizes the turbulent kinetic energy content for any subset of the base. In other words, the POD modes provide a least-order expansion of the fluctuating flow field, such as

$$\mathbf{v}(\mathbf{x},t) = \sum_{j=1}^{N} a_j(j)\Phi_j(\mathbf{x}) + \mathbf{v}_{res}(\mathbf{x},t), \tag{2}$$

by minimizing the residual $\mathbf{v}_{res}$. The $a_j(t)$ are called temporal POD coefficients, while $\Phi_j(\mathbf{x})$ are the spatial POD modes or simply POD modes.

The POD approach provides an orthogonal set of spatial and temporal modes that are energy ranked. The spatial modes $\Phi_j(\mathbf{x})$ provide the shape of the mode, while the Fourier spectra of the POD coefficients $a_j(t)$ readily reveal any dominant frequencies related to these modes. In the case of a coherent fluctuation in the flow field, the oscillating global mode is usually captured by two modes [17] of similar coherent kinetic energy, of the same dominant frequency, and with a corresponding spatial shape. If such two modes are encountered, the coherent velocity fluctuation $\mathbf{v}^c$ can be reconstructed from the POD modes.

$$\mathbf{v}^c(\mathbf{x},t) = \Re\left[\overline{\sqrt{a_j^2 + a_k^2}}\left(\mathbf{\Phi}_j(\mathbf{x}) + i\mathbf{\Phi}_k(\mathbf{x})\right)\mathrm{e}^{-i\omega t}\right] \tag{3}$$

The frequency ω of the global mode is obtained from the spectra of the time coefficients (a_j and a_k) of the two POD modes j and k describing the global mode.

2.2. Physical mode construction using linear stability analysis

The approach to physically construct the coherent fluctuations is fundamentally different from the empirical technique. For the physical reconstruction the concept of linear hydrodynamic stability analysis is employed. The starting point for the stability analysis are the incompressible Navier-Stokes equation and the incompressible continuity equation (Eqn. 5), reading

$$\frac{\partial \mathbf{v}}{\partial t} + \mathbf{v}\cdot\nabla\mathbf{v} = -\frac{1}{\rho}\nabla p + \frac{1}{Re}\nabla^2\mathbf{v} \tag{4}$$

$$\nabla\cdot\mathbf{v} = 0. \tag{5}$$

Subsequently, the triple decomposition ansatz (1) is substituted into the Navier-Stokes equation 4 and the incompressible continuity equation (5). By time-averaging one obtains the governing equations for the mean field:

$$\mathbf{V}\nabla\mathbf{V} = -\frac{1}{\rho}\nabla P + \frac{1}{Re}\nabla^2\mathbf{V} - \nabla\cdot\left(\overline{\mathbf{v}^c\mathbf{v}^c} + \overline{\mathbf{v}^s\mathbf{v}^s}\right) \tag{6}$$

$$\nabla\cdot\mathbf{V} = 0. \tag{7}$$

The term $-\nabla\cdot\left(\overline{\mathbf{v}^c\mathbf{v}^c} + \overline{\mathbf{v}^s\mathbf{v}^s}\right)$ determines how the mean flow field is changed by the stochastic and coherent Reynolds stresses. Thus, if the analysis is carried out on the measured mean flow fields at the limit-cycle oscillation, the mean-coherent and the mean-turbulent interactions are already reflected in the mean flow field. The governing equations for the coherent fluctuations are obtained by subtracting the time-averaged equations of motion from the phase-averaged equations [20]. The continuity equation has to be fulfilled for each component.

$$\frac{\partial \mathbf{v}^c}{\partial t} + \mathbf{v}^c\cdot\nabla\mathbf{V} + \mathbf{V}\cdot\nabla\mathbf{v}^c = -\frac{1}{\rho}\nabla p^c + \frac{1}{Re}\nabla^2\mathbf{v}^c - \nabla\cdot\left(\tau^R + \tau^N\right) \tag{8}$$

$$\nabla\cdot\mathbf{v}^c = 0 \tag{9}$$

The non-linear term $\tau^N = \mathbf{v}^c\mathbf{v}^c - \overline{\mathbf{v}^c\mathbf{v}^c}$ is neglected in the following assuming small-amplitude perturbations. The remaining term $\tau^R = \langle\mathbf{v}^s\mathbf{v}^s\rangle - \overline{\mathbf{v}^s\mathbf{v}^s} = \widetilde{\mathbf{v}^s\mathbf{v}^s}$ is the difference between the phase-average and the time-average of the stochastic Reynolds stresses. It can be regarded as the oscillation of the stochastic Reynolds stresses due to the passage of the coherent perturbation [20]. To implement these stresses, one has to find an appropriate model. Here, a Newtonian eddy viscosity model is employed

$$\tau^R = -\widetilde{u_i'u_j'} = \nu_t\left(\frac{\partial u_i^c}{\partial x_j} + \frac{\partial u_j^c}{\partial x_i}\right). \tag{10}$$

The indices $i, j = 1, 2, 3$ represent the three velocity components and ν_t is the eddy viscosity of the unperturbed flow[22].

To model these stresses, the eddy viscosity has to be estimated from the experimental results. For a three-dimensional flow, as the swirling jet, the turbulence is not isentropic. An optimal representation of ν_t is obtained using a least-square fit over all resolved Reynolds stresses[23]

$$\nu_t = \frac{\left(-\overline{u_i' u_j'} + \frac{2}{3}k\delta_{ij}\right) \cdot \left(\frac{\partial U_j}{\partial x_i} + \frac{\partial U_i}{\partial x_j}\right)}{\left(\frac{\partial U_k}{\partial x_l} + \frac{\partial U_l}{\partial x_k}\right) \cdot \left(\frac{\partial U_k}{\partial x_l} + \frac{\partial U_l}{\partial x_k}\right)}, \tag{11}$$

with the summation over the repeating indices i, j, k, and $l = 1 - 3$. Subsequently, the eddy-viscosity ν_t is lumped into the Reynolds number ($Re_{\nu_t} = \frac{U_0 D_h}{\nu + \nu_t}$)) and the classical Orr-Sommerfeld equation is obtained

$$\frac{\partial \mathbf{v}^c}{\partial t} + \mathbf{v}^c \cdot \nabla \mathbf{V} + \mathbf{V} \cdot \nabla \mathbf{v}^c = -\frac{1}{\rho}\nabla p^c + \frac{1}{Re_{\nu_t}}\nabla^2 \mathbf{v}^c. \tag{12}$$

2.2.1. Local analysis

In the local linear stability concept, the flow field is sliced into velocity profiles and the solution to Eqn. 12 is searched for at each axial location separately. The advantage of this strategy is the drastic reduction in terms of computational costs. However, this approach is, in principal, only valid if the flow under consideration is strictly parallel. In contrast to this, the velocity fields of a swirling jet undergoing vortex breakdown exhibit a strong nonparallelism in the vortex breakdown region. Nevertheless, very good results were achieved with the local analysis of significantly nonparallel flow (see e.g., Ref.[24]).

The treatment of the flow to be weakly nonparallel allows for the decomposition of the coherent fluctuations into normal modes, which are periodic in time and space.

$$\mathbf{v}^c(\mathbf{x}, t) = \Re\left[\hat{\mathbf{v}}(r) \mathrm{e}^{i(\alpha x + m\theta - \omega t)}\right] \tag{13}$$

Here, α is the complex streamwise wave number, ω the complex frequency, m the real azimuthal wave number, $\hat{\mathbf{v}}$ the radial amplitude function, and $\Re$ refers to the real part.

For a given mean velocity profile, equations (9, 12, 13) can be transformed with the appropriate boundary conditions[25] into an eigenvalue problem

$$\mathbf{A}(\alpha)\phi = \omega \mathbf{B}(\alpha)\phi. \tag{14}$$

If one is interested in the propensity of the flow to feature self-excited oscillations, Eqn. 14 has to be solved for complex ω at a given complex α, the so-called spatio-temporal analysis. It allows for the important distinction between a convectively unstable instability and an absolutely unstable instability. Only an absolute instability can grow up- and downstream of its origin and contaminate the entire flow in the limit of infinite time. To determine the absolute/convective nature of an instability, on has to look for the temporal growth rate of the wavepacket with vanishing group speed[26]. Mathematically, this corresponds to the search for saddlepoints in the complex α-ω plane, where the functional $F = (\partial\omega_i/\partial\alpha_r)^2 + (\partial\omega_i/\partial\alpha_i)^2$ has a local minimum. The frequency at a saddle point is called the absolute frequency. If $\omega_{0,i} < 0$ the parallel flow profile is convectively unstable, if $\omega_{0,i} > 0$ the flow is absolutely unstable.

It was shown for wake flows, as in the present study, that the limit-cycle oscillation is most accurately predicted if the stability analysis is carried out on the mean flow field[27,28]. A necessary condition for the flow to be linearly globally unstable is the existence of a region of absolute instability, which is sufficiently long[29]. If such a region of absolute instability is present, one can derive the global instability from the local analysis. A criterion for the linear global mode's frequency ω_g is given by the saddle point criterion[29]

$$\omega_g = \omega_0(x_s) \quad \text{with} \quad \frac{d\omega_0}{dx}(x_s) = 0. \tag{15}$$

This criterion is generally not fulfilled along the real x-axis, since the real and imaginary part of the ω_0 do not necessarily have their maxima at the same x location. Therefore, in order to fulfill the saddle point criterion the

Table 1: Operating conditions of the investigated cases.

Flame type	$\frac{T_{\text{in}}}{1\text{K}}$	$\frac{T_{\text{ad}}}{1\text{K}}$	ϕ	Ω	$\frac{u_0}{1\text{m/s}}$	PVC
Detached	620	1850	0.8	0.2	72.9	PVC at $St = 0.11$
Trumpet	620	1850	0.68	0.1	69.6	PVC at $St = 0.056$
V flame	620	1850	0.56	0	66.1	No PVC

absolute growth rate curve is continued analytically into the complex X-plane. This can be accomplished by fitting a rational polynomial to the curve on the real x-axis and evaluating it in the complex X-plane. The real part of the frequency at this saddle point determines the frequency and the imaginary part the growth rate of the global mode. If $\omega_{g,i} > 0$, the flow is globally unstable, oscillating at $\omega_{g,r}$ while the flow is globally stable for $\omega_{g,i} < 0$.

Once the global frequency is determined, $\mathbf{v}^c$ can be reconstructed by solving the system of equations (9, 12, and 13) with $\omega = \omega_{g,r}$. The spatial shape of the global mode $\mathbf{v}^c$ is calculated from the local amplitude functions $\hat{\mathbf{v}}$ by integrating the spatial growth rates (α) from a spatial local analysis.

$$\mathbf{v}^c(\mathbf{x}, t) = \Re\left[A_0 \hat{\mathbf{v}}(\mathbf{x}) \mathrm{e}^{i\left(\int_0^x \alpha(\xi) d\xi + m\theta - \omega t\right)}\right] \tag{16}$$

The numerical implementation of the solution of the eigenvalue problem closely follows the implementation presented in Refs.[17,18]. The Orr-Sommerfeld operator is discretized using a Chebyshev pseudospectral collocation technique[25] and the eigenvalueproblem is solved using the MATLAB$^{\text{TM}}$ routine EIG. Once the suitable eigenvalue and eingenmode have been identified, it is efficiently tracked using the MATLAB$^{\text{TM}}$ Arnoldi-iteration-based routine EIGS. A detailed description of the numerical approach is provided in the work of Oberleithner and coworkers[17,18].

2.2.2. Global analysis

In the global analysis a perturbation of the form:

$$\mathbf{v}^c(\mathbf{x}, t) = \Re\left[\hat{\mathbf{v}}(x, r) \mathrm{e}^{i(m\Theta - \omega_g t)}\right]. \tag{17}$$

is used, where $\hat{\mathbf{v}}(x, t)$ is the vector of the two-dimensional amplitude functions. In the present temporal framework, the complex eigenvalue ω_g, and the associated eigenvectors $\hat{\mathbf{v}}$ are sought. The resulting three-dimensional partial derivative GEVP is linear on the eigenvalue ω_g and is written as follows:

$$\mathbf{A}\hat{\mathbf{q}} = \omega_g \mathbf{B}\hat{\mathbf{q}}. \tag{18}$$

The elliptic eigenvalue problem (18) must be complemented with adequate boundary conditions for the disturbance variables. In streamwise direction, homogeneous Neumann conditions are imposed at the inlet and homogeneous Dirichlet conditions at the walls. The decay of perturbations is imposed through a sponge region at the outlet to avoid spurious reflections. These sponge regions consist of very low local Reynolds numbers, being 80 to 90% lower than the surrounding Reynolds numbers. The same technique has been successfully used by Meliga et al.[30] for recovering the global modes of swirling jets. At the radial axis $r = 0$, the same boundary conditions are applied, as for the local analysis according to Ref. [25].

Subsequently, the elliptic global problem, written as a GEVP (18) is solved using an Arnoldi algorithm. Details about the employed numerical methods and the discretization scheme can be found in the literature (e.g., Ref.[31]) and in the work of Paredes et al.[32].

3. Experimental observations

The reacting swirling jets under investigation are created in a swirl-stabilized model combustor, as depicted in Fig. 1a. It consists of an adjustable radial swirl generator, an annular duct, and a quartz glas combustion chamber with a diameter of 200 mm, a length of 300 mm and an open exit boundary. The outer diameter of the annular duct of

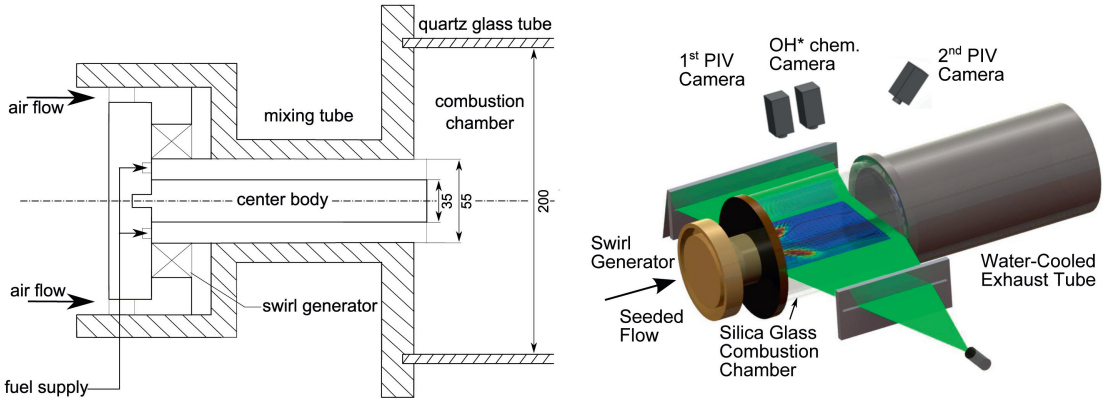

(a) Generic swirl stabilized combustor.

(b) Sketch of the combustor test rig and the experimental setup

Fig. 1: Generic burner and PIV setup.

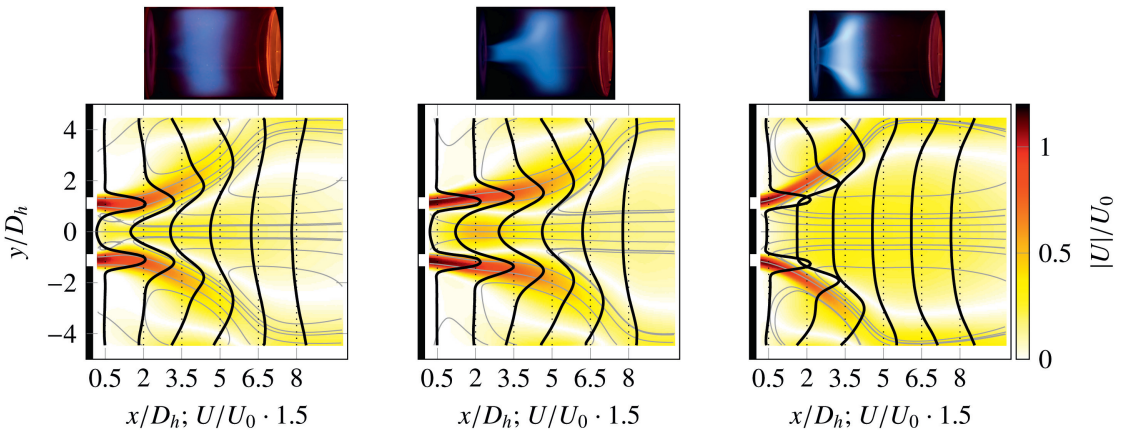

(a) Detached flame

(b) Trumpet flame

(c) V flame

Fig. 2: Streamlines of the time-averaged flow fields superimposed on the normalized axial velocity distribution.

55 mm and the diameter of 35 mm of the centerbody results in an hydraulic diameter of $D_h = 20$ mm. This hydraulic diameter and the bulk velocity in the combustor inlet U_0 are used throughout this work for normalization. Depending on the operating conditions, the Reynolds number of the swirling flow is of the order of 25,000 to 30,000. Thus, the flow is fully turbulent.

The flow measurements are carried out in an atmospheric combustor test-rig at TU Berlin, as shown in Fig. 1b. Stereoscopic high speed particle image velocimetry (S-PIV) at a recording frequency of 3 kHz is employed to resolve all three velocity components in a streamwise sheet aligned with the combustor axis. Therefore, the flow was seeded upstream of the swirl generator with ZrO_2 particles of a nominal diameter of 2 μm. The density field inside the combustor was estimated using a quantitative light sheet (QLS), where the amount of scattered light from the particles is used to recover the planar density distribution. Details about the experimental setup and the measurement uncertainty are provided in a recent publication [13].

During the operation of the combustor, depending on the operating conditions, different flame shapes can be observed. The three most common types are presented in Fig. 2 for the operating conditions provided in Tab. 1. The flame can be detached from the combustor inlet and be located in the downstream section of the combustion chamber. In its second shape the flame is attached to the combustor inlet and shows a trumpet-like shape. Lastly, the flame can

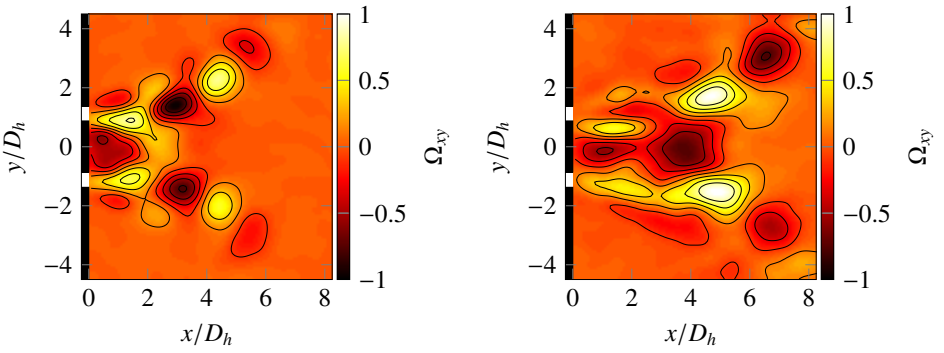

(a) Detached flame (b) Trumpet flame

Fig. 3: Normalized through-plane vorticity Ω_{xy} of the experimentally obtained helical global mode for the detached and the trumpet flame.

also have a very wide opening angle and be attached to combustor inlet. This V-shaped flame is often considered as the standard flame for swirl-stabilized combustion.

The flow fields of the three flames under consideration all show the same general flow topology. It is composed of an emanating jet and large zones of recirculating fluid. An inner recirculation zone (IRZ) is located around the centerline and an outer recirculation zone (ORZ) near the combustor walls. In between the jet and the recirculation zones, highly turbulent shear layers are formed. The flow fields notably differ in terms of the jet divergence and the amount of backflow in the IRZ.

The application of the POD on the measured flow fields provides insight into the presence of the PVC in the different flow fields. Due to space limitations, the outcome is only briefly presented, and for the detailed results of the decomposition the reader is referred to Ref. [13]. For the attached V flame, the POD did not yield any modes corresponding to a self-excited oscillation, such as the PVC. For the detached flame and the trumpet flame, in contrast to that, a strong skew-symmetric, helical oscillation was found. The shape of this oscillation, constructed employing Eqn. 3, is depicted in Fig. 3 at an arbitrary phase. By comparison to previous measurements at isothermal and reacting conditions, the skew-symmetric structures were clearly identified as the PVC[17,13].

4. Results of the local and global stability analysis

The results of the local and global stability analysis are presented in Fig. 4 for the three investigated flow fields. Figure 4a compares the calculated global frequencies ω_g to the experimentally obtained frequencies. The filled markers correspond to the local analysis, where the global frequency is obtained from the local absolute frequencies by the application of Eqn. 15. The vertical dashed lines denote the measured frequencies for the detached flame and the trumpet flame. It can be observed that the frequencies predicted by the local analysis are in reasonable agreement with the measured frequency of the detached flame (approx. 15% deviation) and in excellent agreement with the measured frequency of the trumpet flame (less than 2% deviation). In the case of the attached V flame, the local analysis predicts a positive global growth rate, whereas the experiments showed that the flow is stable. Due to space limitations the local distribution of the complex local absolute frequency ω_0, which determines the global frequency ω_g, is omitted here. For details the reader is referred to Ref. [19].

The hollow markers represent the eigenvalues of the global analysis (Eqn. 18). For the attached V flame, it can be observed that all eigenvalues are stable. Thus, in contrast to the local analysis, the suppression of the PVC in this case is correctly predicted by the global analysis. For the detached flame, the global analysis predicts the most unstable mode at a very similar growth rate and frequency as the local analysis. Similar to the local analysis, the frequency of the instability is underpredicted (approx. 17% deviation). The global analysis of the trumpet flame yields an excellent agreement in terms of the global frequency (less than 3% deviation).

The comparison of the global growth rates and frequencies showed major differences between the results of the local and global analysis of the attached V flame. These are very likely caused by the very strong non-parallelity of

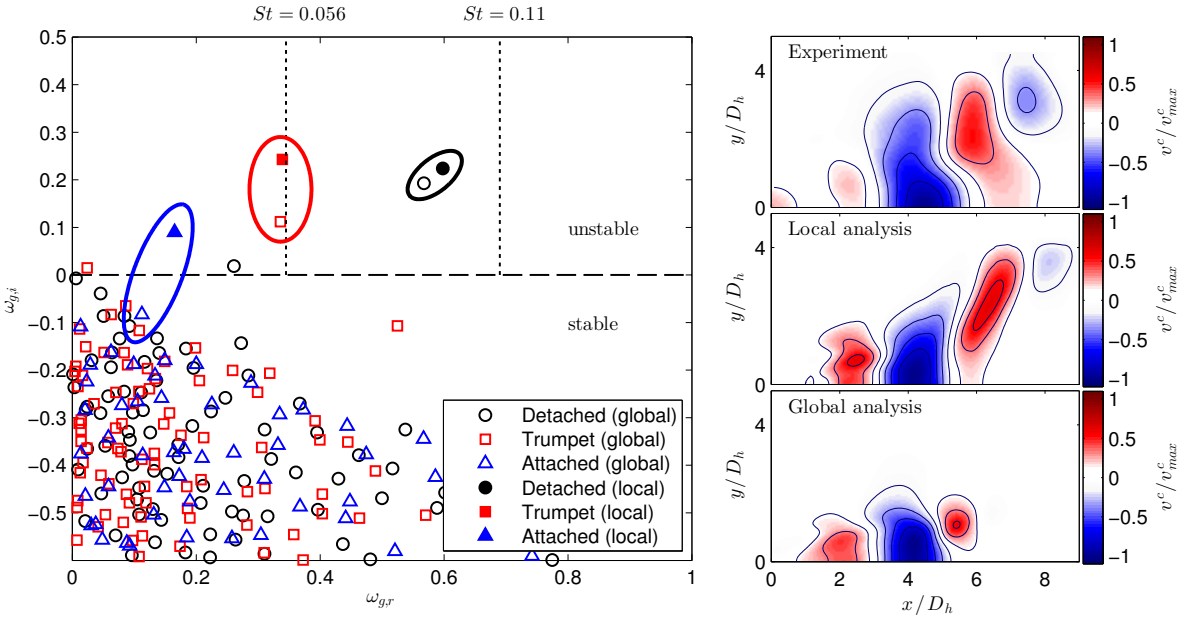

(a) Global frequencies

(b) Global mode shape for trumpet flame

Fig. 4: Predictions of the global stability analysis and comparisons with POD reconstructions of the experimental results.

the flow field of the attached V flame. Consequently, the local analysis, which assumes a quasi-parallel flow, gets increasingly inaccurate and overpredicts the growth rate.

In the case of the detached flame, a reasonable agreement of the local and global analysis to the experimental results is achieved. However, for the global analysis, the results are very sensitive to the selection of the inlet boundary conditions. This is caused by the proximity of the global flow oscillation to the inlet (see Fig. 3) and indicates that for a better match of the frequencies, the flow field upstream of the combustor inlet has to be considered. This could not be done in the present work and has to be postponed to future works.

The analysis of the trumpet flame yields excellent results for both the local analysis and the global analysis. The good quality of the local analysis is presumably related to the very weak non-prallelity of the flow in the region, where the wavemaker is predicted by the local analysis. Furthermore, the structure is sufficiently far away from the inlet, so that the conditions at the inlet are approximated good enough by the imposed boundary conditions.

In summary, the local analysis works best if, as expected, the flow is only weakly non-parallel. The global analysis implements the effect of the non-parallelity but creates additional challenges regarding appropriate boundary conditions in the flow direction, which are not necessary for the local analysis.

Lastly, the spatial structure of the global mode can be obtained from the local and global analysis. While for the global analysis it is readily available as the eigenvector corresponding to the most unstable eigenvalue, in the local analysis, it has to be reconstructed from the eigenvectors of a series of spatial analyses with $\omega = \omega_{g,r}$ (see Eqn. 16).

In Fig. 4b the predicted global mode shapes for the trumpet flame are compared to the experimental result from the POD analysis. The normalized coherent transversal velocity is shown and the phases are adjusted to ease the comparability. Overall, an excellent agreement between the measured and the predicted global mode is evident. Both the local and global analysis predict structures of the correct axial wavelength and with similar spatial distributions.

The high amplitudes of the radial velocity fluctuations on the centerline are planar representations of the precession of the vortex core. The results of the local and the global analysis, thus, unambiguously prove, that the PVC in reacting (and isothermal) combustor flows is caused by a globally unstable hydrodynamic fields. The precession of the vortex core and the axial-radial eddies in the shear layer are two different flow-dynamic features of the same global mode.

5. Summary and conclusions

In the present work the global mode of turbulent reacting swirling jets is experimentally and analytically assessed. This type of flow is of high relevance for the gas turbine industry. Three different cases are considered. If the flame is detached from the combustor inlet, the experiments show a strong periodic oscillation. With the application of proper orthogonal decompositions, the oscillation is related to the well-known single-helical instability, which is known in the combustion community as the precessing vortex core. In the second case, the flame shows a very long trumpet shape and the flow oscillation changes its shape and frequency but remains similarly strong. In the third case, the flame shows an attached V shape and the global flow oscillation is entirely suppressed.

Based on the measured mean flow fields and the estimated density distribution local and global linear stability analyses are carried out. To implement the effect of turbulence on the flow instability, a Newtonian eddy viscosity model is employed. Both the local and the global analysis predict the instability frequency of the detached flame with reasonable accuracy. In the case of the trumpet flame, both analyses yield an excellent agreement to the measurements. In the third considered case, the attached V flame, the local analysis overpredicts the growth rate and yields a global instability, which was not present in the experiments. In contrast to that, the global analysis accurately predicts the suppression of the global mode. Thus, the overprediction of the local analysis is assumed to be caused by the strong non-parallelity of the flow field of the V flame.

Both the local and global analysis are proven to be valuable tools for the analysis of the excitation mechanisms of the PVC and can provide valuable input for the sensible application of active or passive flow control measures. As expected, the gobal analysis has a strong advantage when the flow under consideration is strongly non-parallel. The local analysis, on the other hand, is independent of the streamwise boundary conditions. This can be of a great advantage if only parts of the flow field are accessible to the measurement techniques.

The comparison of the global mode shapes predicted by the local and global analyses to the experiments yields an excellent agreement to the experiments. This proves unambiguously, that the global and local linear stability analyses can reliably capture the correct flow feature and that the PVC and the synchronized Kelvin-Helmhotz instabilities are indeed caused by a globally unstable turbulent flow field and can be interpreted as a global mode that oscillates at its limit-cycle. The improved understanding and the enhanced modeling of the instability form important steps towards the application of theoretically-founded passive and active control strategies.

6. Acknowledgment

The research leading to these results has received funding from the European Research Council under the ERC grant agreement n° 247322, GREENEST.

References

1. Syred, N., Beér, J.M.. Combustion in swirling flows: A review. *Combust Flame* 1974;**23**(2):143–201.
2. Galley, D., Ducruix, S., Lacas, F., Veynante, D.. Mixing and stabilization study of a partially premixed swirling flame using laser induced fluorescence. *Combust Flame* 2011;**158**(1):155–171. doi:10.1016/j.combustflame.2010.08.004.
3. Göckeler, K., Terhaar, S., Paschereit, C.O.. Residence Time Distribution in a Swirling Flow at Nonreacting, Reacting, and Steam-Diluted Conditions. *J Eng Gas Turbines Power* 2013;**136**(041505):1–9. doi:10.1115/1.4026000.
4. Schadow, K.C., Gutmark, E.J.. Combustion instability related to vortex shedding in dump combustors and their passive control. *Prog Energy Combust Sci* 1992;**18**(2):117–132.
5. Paschereit, C.O., Gutmark, E.J., Weisenstein, W.. Excitation of thermoacoustic instabilities by interaction of acoustics and unstable swirling flow. *AIAA J* 2000;**38**(6):1025–1034.
6. Stöhr, M., Boxx, I., Carter, C.D., Meier, W.. Experimental study of vortex-flame interaction in a gas turbine model combustor. *Combust Flame* 2012;**159**(8):2636–2649. doi:10.1016/j.combustflame.2012.03.020.
7. Moeck, J.P., Bourgouin, J.F., Durox, D., Schuller, T., Candel, S.. Nonlinear interaction between a precessing vortex core and acoustic oscillations in a turbulent swirling flame. *Combust Flame* 2012;**159**(8):2650–2668. doi:10.1016/j.combustflame.2012.04.002.
8. Froud, D., O'Doherty, T., Syred, N.. Phase Averaging of the Precessing Vortex Core in a Swirl Burner under Piloted and Premixed Combustion Conditions. *Combust Flame* 1995;**100**(3):407–412.
9. Roux, S., Lartigue, G., Poinsot, T., Meier, U., Bérat, C.. Studies of mean and unsteady flow in a swirled combustor using experiments, acoustic analysis, and large eddy simulations. *Combust Flame* 2005;**141**(1-2):40–54. doi:10.1016/j.combustflame.2004.12.007.
10. Giauque, A., Selle, L., Gicquel, L.Y., Poinsot, T., Buechner, H., Kaufmann, P., et al. System identification of a large-scale swirled partially premixed combustor using LES and measurements. *J Turbul* 2005;**6**:N21. doi:10.1080/14685240512331391985.

11. Syred, N.. A review of oscillation mechanisms and the role of the precessing vortex core (PVC) in swirl combustion systems. *Prog Energy Combust Sci* 2006;**32**(2):93–161. doi:10.1016/j.pecs.2005.10.002.
12. Boxx, I., Arndt, C.M., Carter, C.D., Meier, W.. High-speed laser diagnostics for the study of flame dynamics in a lean premixed gas turbine model combustor. *Exp Fluids* 2010;**52**(3):555–567. doi:10.1007/s00348-010-1022-x.
13. Terhaar, S., Oberleithner, K., Paschereit, C.O.. Impact of Steam-Dilution on the Flame Shape and Coherent Structures in Swirl-Stabilized Combustors. *Combust Sci Technol* 2014;**186**:889–911. doi:10.1080/00102202.2014.890597.
14. Kuenne, G., Ketelheun, A., Janicka, J.. LES modeling of premixed combustion using a thickened flame approach coupled with FGM tabulated chemistry. *Combust Flame* 2011;**158**(9):1750–1767. doi:10.1016/j.combustflame.2011.01.005.
15. Liang, H., Maxworthy, T.. An experimental investigation of swirling jets. *J Fluid Mech* 2005;**525**:115–159. doi:10.1017/S0022112004002629.
16. Gallaire, F., Ruith, M.R., Meiburg, E., Chomaz, J.M., Huerre, P.. Spiral vortex breakdown as a global mode. *J Fluid Mech* 2006; **549**:71–90. doi:10.1017/S0022112005007834.
17. Oberleithner, K., Sieber, M., Nayeri, C.N., Paschereit, C.O., Petz, C., Hege, H.C., et al. Three-dimensional coherent structures in a swirling jet undergoing vortex breakdown: stability analysis and empirical mode construction. *J Fluid Mech* 2011;**679**:383–414. doi:10.1017/jfm.2011.141.
18. Oberleithner, K., Terhaar, S., Rukes, L., Paschereit, C.O.. Why Non-Uniform Density Suppresses the Precessing Vortex Core. *J Eng Gas Turbines Power* 2013;**135**(121506):1–9.
19. Terhaar, S., Oberleithner, K., Paschereit, C.O.. Key parameters governing the precessing vortex core in reacting flows: An experimental and analytical study. *Proc Combust Inst* 2014;doi:10.1016/j.proci.2014.07.035.
20. Reynolds, W.C., Hussain, A.K.M.F.. The mechanics of an organized wave in turbulent shear flow. Part 3. Theoretical models and comparisons with experiments. *J Fluid Mech* 1972;**54**(02):263–288. doi:10.1017/S0022112072000679.
21. Berkooz, G., Holmes, P., Lumley, J.L.. The Proper Orthogonal Decomposition in the Analysis of Turbulent Flows. *Annu Rev Fluid Mech* 1993;**25**(1):539–575. doi:10.1146/annurev.fl.25.010193.002543.
22. Reau, N., Tumin, A.. On harmonic perturbations in a turbulent mixing layer. *Eur J Mech - B/Fluids* 2002;**21**(2):143–155. doi:10.1016/S0997-7546(01)01170-0.
23. Ivanova, E.M., Noll, B.E., Aigner, M.. A Numerical Study on the Turbulent Schmidt Numbers in a Jet in Crossflow. *J Eng Gas Turbines Power* 2012;**135**(1):011505. doi:10.1115/1.4007374.
24. Pier, B.. Local and global instabilities in the wake of a sphere. *J Fluid Mech* 2008;**603**:39–61. doi:10.1017/S0022112008000736.
25. Khorrami, M., Malik, M., Ash, R.. Application of spectral collocation techniques to the stability of swirling flows. *J Comput Phys* 1989; **81**(1):206–229.
26. Briggs, R.. *Electron-stream interaction with plasmas*. MIT Press, Cambridge,Massachusetts.; 1964. URL: `http://www.getcited.org/pub/101205944`.
27. Barkley, D.. Linear analysis of the cylinder wake mean flow. *Europhys Lett* 2006;**75**(5):750–756. doi:10.1209/epl/i2006-10168-7.
28. Pier, B.. On the frequency selection of finite-amplitude vortex shedding in the cylinder wake. *J Fluid Mech* 2002;**458**:407–417. doi:10.1017/S0022112002008054.
29. Chomaz, J.M., Huerre, P., Redekopp, L.G.. A frequency selection criterion in spatially developing flows. *Stud Appl Math* 1991;**84**:119–144.
30. Meliga, P., Gallaire, F., Chomaz, J.M.. A weakly nonlinear mechanism for mode selection in swirling jets. *J Fluid Mech* 2012;**699**:216–262. doi:10.1017/jfm.2012.93.
31. Theofilis, V.. Advances in global linear instability analysis of nonparallel and three-dimensional flows. *Prog Aerosp Sci* 2003;**39**(4):249–315. doi:10.1016/S0376-0421(02)00030-1.
32. Paredes, P., Hermanns, M., Le Clainche, S., Theofilis, V.. Order 104 speedup in global linear instability analysis using matrix formation. *Comput Methods Appl Mech Eng* 2013;**253**:287–304. doi:10.1016/j.cma.2012.09.014.